Int. J. Electrochem. Sci., 15 **(2020)** 8892 – 8900, doi: 10.20964/2020.09.33

International Journal of
ELECTROCHEMICAL
SCIENCE
www.electrochemsci.org

Short Communication

Ultrafine Tin Dioxide Nanoparticles Grown on Nitrogen-doped Graphene with Rich Pyrrolic Nitrogen for Excellent Supercapacitor Performance

Gaosheng Nie[1,*], *Shizhen Dai*[2], *Hangchun Deng*[2], *Chunyan Wang*[2]

[1] School of Internet of Things, Jiangxi Teachers College, YingTan, Jiangxi, 335000, China
[2] East China University of Technology, Nanchang, Jiangxi, 330013, China
[*]E-mail: n18970187308@163.com

Received: 7 May 2020 / *Accepted:* 8 July 2020 / *Published:* 10 August 2020

Composites of ultrafine tin dioxide nanoparticles grown on nitrogen-doped graphene (SnO_2@NG) with high pyrrolic nitrogen content are successfully prepared via a one-step method by employing graphene oxide, tin chloride, and urea as raw materials. Morphology and microstructure of SnO_2@NG are characterized by transmission electron microscopy (TEM), X-ray photoelectron spectroscopy (XPS), and thermogravimetric analysis (TGA), revealing evenly dispersed SnO_2 nanoparticles on the surface of nitrogen-doped graphene sheets and a SnO_2 content of 54.23%. The SnO_2@NG electrode exhibits a specific capacitance of 289.5 F/g at a current density of 0.5 A/g in 0.5 mol/L Na_2SO_4 solution and retains 92.85% of its initial capacitance after 2000 charge/discharge cycles. These results prove that SnO_2@NG is an excellent material for high-performance supercapacitors.

Keywords: tin dioxide, nitrogen-doped graphene, supercapacitors.

1. INTRODUCTION

The demand for energy has grown in the past few decades, and concerns about environmental issues have accelerated the development of energy storage and energy conversion devices [1]. Supercapacitors, also known as electrochemical capacitors, have the advantages of high power density, light weight, small size, and long cycle life [2] and are considered to be one of the most promising energy conversion/storage systems to meet energy storage needs in the future [3-5]. No other electric energy storage device, such as capacitors, electrostatic capacitors, electrolytic capacitors, and ceramic capacitors, has comparable characteristics [6]. Currently, supercapacitors are used in hybrid vehicles, mobile electronics, and medical systems. At present, the hotspot of supercapacitor research is the development of new electrode materials to increase specific power and energy density and reduce

manufacturing costs [7, 8].

Generally, the electrode material is the main factor that affects the electrochemical performance of supercapacitors. At present, metal oxides [9], conductive polymers [10], and carbonaceous materials [11] are the three most promising electrode materials for high-performance supercapacitors.

Carbon-based materials, including activated carbon [12, 13], xerogel [14], carbon nanotubes [15,16], porous carbon [17], graphene [18-20], and others, are often used as electrode materials due to their excellent electrical conductivity, high specific surface area (SSA), and good mechanical properties. In addition, conductive polymers and transition metal oxides are two typical pseudocapacitive materials that can store more charge than carbon materials. Single carbon materials tend to agglomerate and accumulate [21], resulting in limited applications as supercapacitors. Compared with single electrode materials, the addition of metal oxide-based materials, such as RuO_2 [22], MnO_x [23-25], CoO_x [26], SnO_2 [27], and other pseudo-capacitors, has attracted wide attention due to these materials' high optical transparency, electrical conductivity, high theoretical capacity, low cost, and good environmental compatibility, with SnO_2 exhibiting outstanding properties. In addition, doping nano-carbide with one or two heteroatoms (such as nitrogen, boron, iodine, sulfur, and phosphorus) improves the capacitance and forms active sites during the electrochemical process [28, 29].

In this work, SnO_2@NG composites of well-dispersed SnO_2 particles and with high content of pyrrolic nitrogen have been prepared to induce a synergistic effect for a boosted supercapacitor performance. SnO_2@NG exhibited a specific capacitance of 289.5 F/g at 0.5 A/g in neutral solution and revealed to be an ideal electrode material with high capacitance retention and good cycling stability.

2. EXPERIMENTAL

2.1. Chemicals

Urea and ethylene glycol (EG) were obtained from Sigma-Aldrich. $SnCl_2{\cdot}H_2O$, Na_2SO_4, ethyl alcohol, and dimethylformamide (DMF) were obtained from China Medicine Co. All reagents were of analytical grade and used without further purification.

2.2. Synthesis of tin dioxide / nitrogen-doped graphene (SnO_2@NG)

First, 100 mg of graphene oxide (GO) was added to 100 mL of ethylene glycol and ultrasonically dispersed for 2 h to obtain a stable GO suspension. Then, 0.4 mg of $SnCl_2 \cdot H_2O$ and 100 mg of urea were added, and the resulting mixture was poured into a round bottom flask at 198 °C and refluxed for 8 h. After the reaction was completed, the obtained black solid product was filtered and washed with deionized water and ethanol three times each. Finally, the product was vacuum dried at 80 °C and annealed in an argon atmosphere at 500 °C for 2 h. Pure nitrogen-doped graphene (NG) was prepared in the same way without the addition of $SnCl_2{\cdot}H_2O$.

2.4. Electrochemical characterization

Electrochemical tests were performed on a CHI660E electrochemical workstation with a three-electrode system in a 0.5 M Na_2SO_4 electrolyte solution. A saturated calomel electrode (SCE) and platinum wire were used as the reference electrode and counter electrode, respectively. The working electrode was made of the active substance (NG or SnO_2@NG), PTFE, and carbon black, and the mass ratio was 85:5:10. This compound mixture was then pressed onto Ni foam (1×1.5 cm^2) and dried under vacuum. The electrochemical properties of the obtained working electrode were analyzed by cyclic voltammetry (CV) and constant current charge/discharge (GCD). Specific capacitances Cs were calculated from the constant current charge/discharge curve using eq. (1)

$$C = I \cdot t/m \cdot \Delta U \quad (1)$$

where I stands for the discharge current, t for the discharge time, m for the mass of the active substance, and ΔU for the voltage window.

2.4. Materials characterization

TEM and high-resolution TEM (HRTEM) images were obtained using a JEM-2100F transmission electron microscope. XPS analysis was carried out on a Thermo Fisher X-ray photoelectron spectrometer (Al Kα radiation source). TGA analysis was performed using a thermogravimetric analyzer.

3. RESULTS AND DISCUSSION

3.1. Morphostructural characterization of nanomaterials

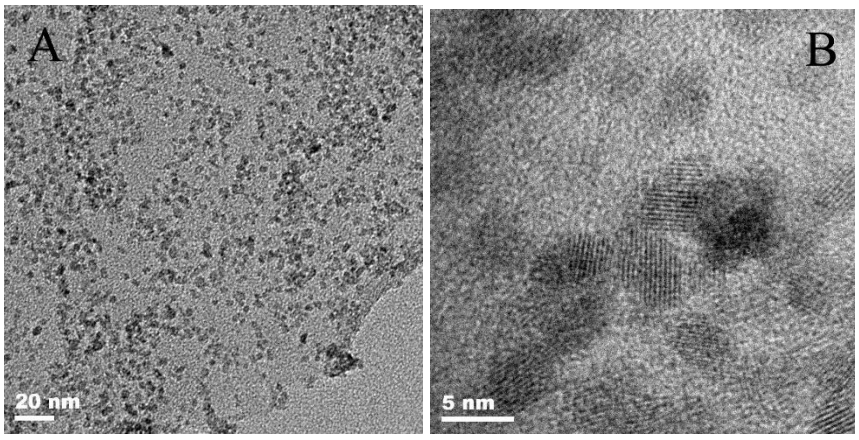

Figure 1. (A) TEM and (B) HRTEM image of SnO_2@NG.

Figure 1 shows the TEM and HRTEM images of SnO_2@NG. The TEM image reveals that the SnO_2 nanoparticles were uniformly dispersed on the surface of the NG sheets (Figure 1A), and the

HRTEM image shows a clear lattice and an excellent crystal structure (Figure 1B). The SnO_2 nanoparticles were very small with a size of about 3–6 nm, and the lattice spacing was 0.3–0.4 nm. In addition, SnO_2 nanoparticles showed no obvious agglomeration and were attached to the surface of the NG sheets, which were uniformly dispersed and stable. This may be attributed to the fact that NG sheets can effectively prevent SnO_2 nanoparticle agglomeration during the preparation.[30]

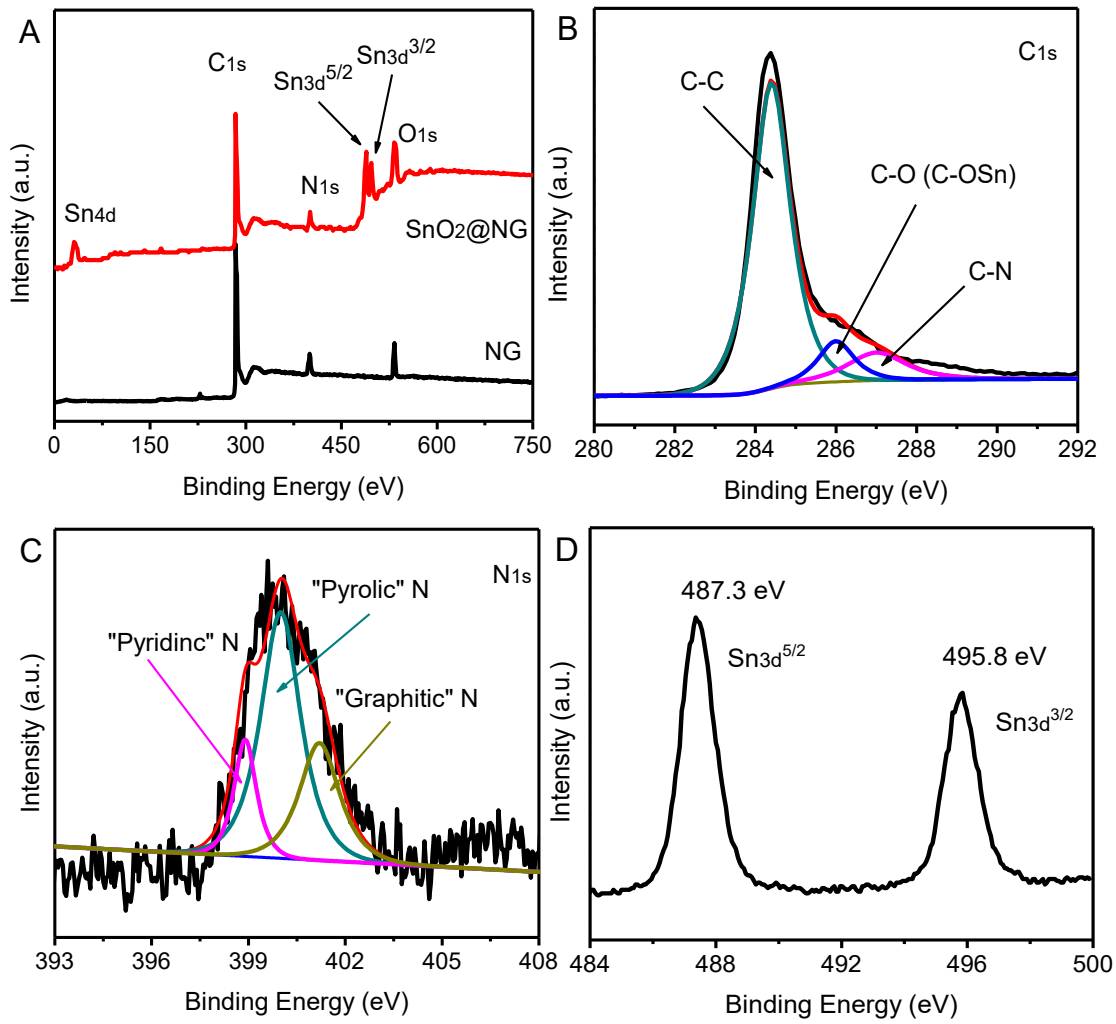

Figure 2. (A) XPS survey spectra of NG and SnO_2@NG; high-resolution XPS spectra of SnO_2@NG: (B) C 1s, (C) N 1s, and (D) Sn 3d region.

XPS spectroscopy was applied to further confirm the chemical compositions and chemical structures of NG and SnO_2@NG. Figure 2A shows the full XPS spectra of NG and SnO_2@NG, revealing three strong characteristic peaks for NG at 532.2, 400, and 284.6 eV, corresponding to O 1s, C 1s, and N 1s, respectively.[31] The XPS spectrum of SnO_2@NG shows three additional peaks corresponding to Sn 4d (24.8 eV), Sn $3d^{5/2}$ (487.3 eV), and Sn $3d^{3/2}$ (495.8 eV), indicating that SnO_2 particles were anchored to the surface of NG.[32]

High-resolution XPS spectra of O 1s, C 1s, N 1s, and Sn 3d were obtained by XPS peak splitting. The peaks at 284.3, 286, and 287.2 eV in Figure 2B were assigned to the characteristic peaks

of C–C, C–O (C–O–Sn), and C–N [33, 34] and confirm the doping of N and Sn into the NG sheets. The nitrogen doping level was obtained by deconvolution of the N 1s spectrum into three different peaks (Figure 2C), indicating that the N atoms in SnO_2@NG exhibit three different valence states of pyridinic N (398.4 eV), pyrrolic N (399.8 eV), and graphitic N (401.4 eV). In general, pyrrolic N and pyridinic N increase the pseudocapacitance through redox reactions, while graphitic N increases the conductivity of carbon-based materials [35]. Notably, pyrrolic N is the dominant species in SnO_2@NG and effectively increases the pseudocapacitance of SnO_2@NG. Figure 2D shows the Sn 3d high-resolution spectrum of SnO_2@NG with the characteristic peaks of Sn $3d^{5/2}$ and Sn $3d^{3/2}$ at 487.3 and 495.8 eV, respectively, which is in good agreement with previously reported data of the SnO_2 phase [36].

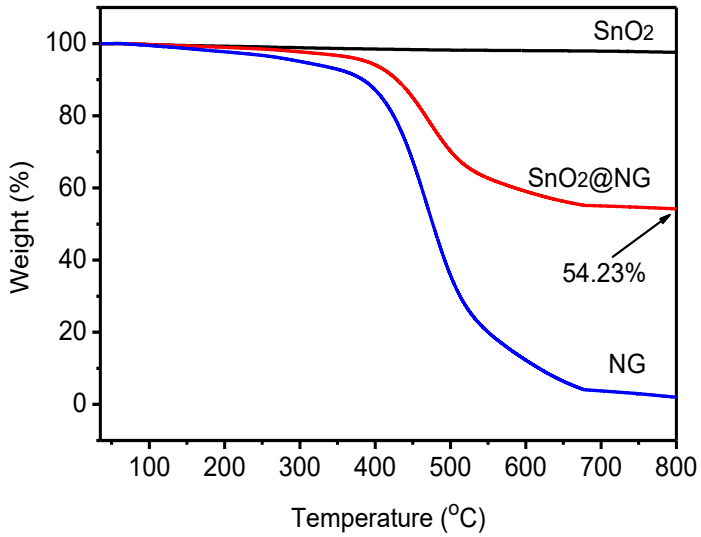

Figure 3. TGA curves of bare SnO_2, SnO_2@NG, and pure NG in air atmosphere.

TGA is an effective method to investigate the composition of composite materials. [37] The SnO_2 content in the SnO_2@NG composite was determined by TGA in an air atmosphere. The TGA curves of SnO_2, NG, and SnO_2@NG are shown in Figure 3, revealing that the mass loss of SnO_2 throughout the process is negligible. NG and SnO_2@NG showed a slight mass loss in the range of 100–400 °C due to the decomposition of a small amount of oxygen-containing functional groups of NG. Temperature increase starting at 400 °C resulted in a violent reaction between the NG sheets and oxygen in the air to generate carbon monoxide and carbon dioxide, rapidly increasing the weight loss rate of the sample. At temperatures in the range of 700–800 °C, nitrogen-doped graphene combustion took place, and only SnO_2 remained in SnO_2@NG. Comparison of the weight losses of SnO_2, NG, and SnO_2@NG showed that the SnO_2 content in SnO_2@NG was 54.23 wt%.

3.2. Electrochemical Performance

Cyclic voltammetry (CV) was performed to characterize the electrical properties of NG and the SnO_2@NG composite in 0.5 mol/L Na_2SO_4 solution, as shown in Figure 4. The CV curve of NG was almost rectangular, which is characteristic for a typical electrical double layer capacitor (EDLC), indicating that NG has a good EDLC performance. The CV curve of SnO_2@NG was pseudo-rectangular, showing that the SnO_2@NG composite has EDLC and Faraday pseudocapacitance features.[38] Moreover, the SnO_2@NG electrode exhibited a larger area under the CV curve, indicating that the composite's capacitance is much higher than that of free NG [39]. This can be attributed to the pseudocapacitance of the SnO_2 phase and the intrinsic capacitance of NG, which synergistically enhance the electrochemical performance of the SnO_2@NG composite.

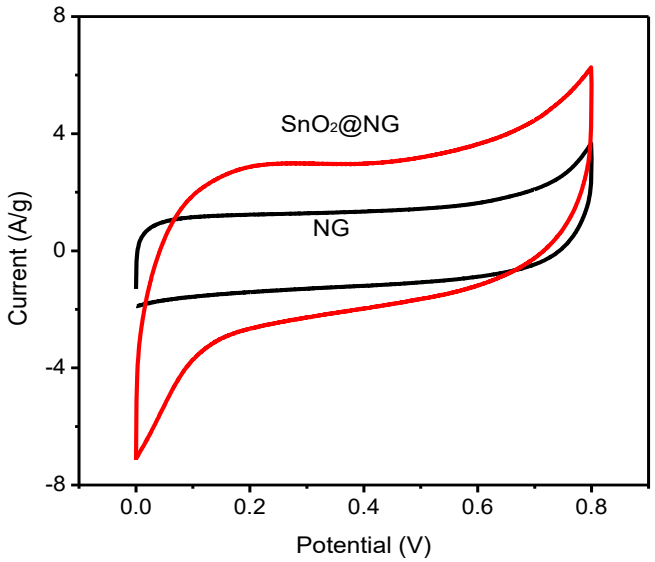

Figure 4. CVs of NG and SnO_2@NG in 0.5 mol/L Na_2SO_4 solution at 20 mV/s.

Figure 5A,B display the GCD curves of NG and the SnO_2@NG composite at various current densities. Obviously, the shape of the isosceles triangle remained unchanged, indicating that both NG and SnO_2@NG electrodes exhibited a charge/discharge performance with good reversibility [40].

The specific capacitances Cs of NG and SnO_2@NG were calculated from the discharge curves according to the equation $Cs = I \times \Delta t / (\Delta U \times m)$. At 0.5 A/g, the gravimetric Cs was 289.5 F/g for SnO_2@NG and 160.2 F/g for NG, which proves that the pseudocapacitance of the SnO_2 nanoparticles considerably enhanced the Cs values.

The diagram shown in Figure 5C compares the Cs values of NG and SnO_2@NG at various current densities. The specific capacitances of SnO_2@NG were calculated to be 289.4, 280.5, 271.7, 265.1, and 254.0 F/g at 0.5, 1, 2, 3, and 5 A/g, respectively. The corresponding specific capacitance retention rates were 100%, 96.9%, 93.9%, 91.6%, and 87.8%, respectively. These results indicate that the SnO_2@NG composite has an excellent rate performance and qualifies as an ideal super-grade capacitor electrode material.

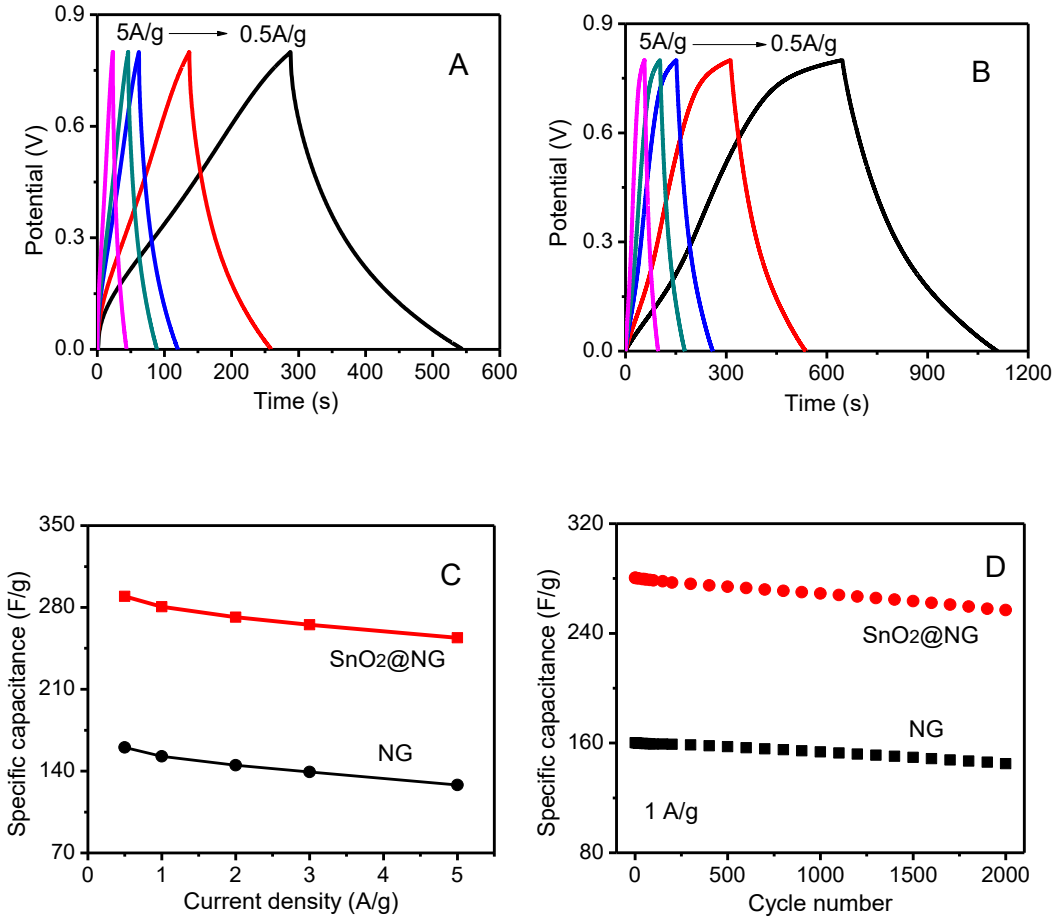

Figure 5. Charge/discharge curves of NG (A) and SnO_2@NG (B) at different current densities from 0.5 to 10 A/g; (C) specific capacitances Cs calculated from the GCD curves; (D) cycling stabilities of NG and SnO_2@NG electrodes in 0.5 M Na_2SO_4 electrolyte at 1 A/g.

High cycling stability is very important for the application of supercapacitors. The cycling stabilities of the NG and SnO_2@NG composite electrodes were tested at 1 A/g over 2000 cycles, and the results are displayed in Figure 5D. The Cs of the SnO_2@NG electrode decreased from 289.4 to 268.7 F/g after 2000 cycles, corresponding to a capacitance retention of 92.85%. For comparison, the Cs retention of NG was only 90.6%. This remarkable capacitance retention may be attributed to the fact that NG sheets suppress the aggregation of SnO_2 during cycling.[30]

To assess the capacitive performance of SnO_2@NG, the specific capacitances measured in this work were compared with those of similar materials reported recently. As shown in Table 1, the SnO_2@NG electrode exhibited the highest Cs among the listed SnO_2-based electrode materials. This superior capacitive performance can be attributed to two reasons: (1) NG sheets can suppress the aggregation of SnO_2, resulting in SnO_2 nanoparticle with a large active surface. This structure can accelerate charge transport and facilitate redox reactions.[46] (2) N-doped graphene with high pyrrolic nitrogen content not only provides fast electron transfer channels but also enhances the capacitance.

Table 1. Comparison of Cs of different SnO_2-based electrode materials

Electrode Material	Electrolyte	Cs (F/g)
SnO_2 thin films[41]	1 M KOH	119
SnO_2/MWCNTs[42]	1 M Na_2SO_4	133.33
SnO_2/vulcan carbon[42]	1 M Na_2SO_4	112.14
SnO_2/SWNHs[43]	1 M Na_2SO_4	180.69
Graphene/SnO_2/PEDOT[44]	1M Na_2SO_4	180
SnO_2/CNT[45]	2 M KCl	188.42
SnO_2@NG (this work)	0.5 M Na_2SO_4	289.4

4. CONCLUSIONS

In summary, a SnO_2@NG composite with high pyrrolic nitrogen content was efficiently synthesized via a one-step solvothermal method. The as-prepared composites showed a remarkable electrochemical performance, which was attributed to the well-dispersed SnO_2 nanoparticles anchored to NG sheets. The SnO_2/NG electrode exhibited a high specific capacitance of 289.5 F/g at 0.5 A/g owing to the synergistic effect between the pseudocapacitance of the SnO_2 nanoparticles and the excellent conductivity of the NG sheets. Furthermore, SnO_2@NG exhibited a high capacitance retention rate of 87.7% at 5 A/g and retained 92.85% of its initial capacitance after 2000 charge/discharge cycles. These results prove that the SnO_2@NG composite material has an excellent chemical stability and is an ideal supercapacitor electrode material.

References

1. B.L. Su, Q. Zhang, D. Bonifazi, J. Li, *ChemSusChem*, 4 (2011) 1327.
2. Q. Wang, J. Yan, Z. J. Fan, *Energy Environ. Sci.*, 9 (2016) 729.
3. M. Winter, R.J. Brodd, *Chem.Rev.*, 104 (2004) 4245.
4. H. Zhang, G.P. Cao, Z.Y. Wang, Y.S. Yang, Z.J. Shi, Z.N. Gu, *Nano Lett.*, 8 (2008) 2664.
5. K. Krishnamoorthy, G. K. Veerasubramani, S. Radhakrishnan, S. J. Kim, *Mater. Res. Bull.*, 50 (2014) 499.
6. M. Pumera, *Energy Environ. Sci.*, 4 (2011) 668.
7. L.L. Zhang, R. Zhou , X.S. Zhao, *J. Mater. Chem.*, 20 (2010) 5983.
8. Y. Qian, S.B. Lu, F.L. Gao, *J. Mater. Sci.*, 46 (2011) 3517.
9. B. Huang, C.L. Huang, Y. Qian, *Int. J. Electrochem. Sci.*, 12 (2017) 11171.
10. L.L. Wen, K. Li, J.J. Liu, Y.S. Huang, F.X. Bu, B. Zhao, Y.X. Xu, *RSC Adv.*, 7 (2017) 7688.
11. L. Zheng, K. S. Xia, B. Han, C. G. Zhou, H. Q. Wang, S. Pu, J. P. Wu, *ACS Appl. Nano Mater.*, 1 (2018) 6742.
12. M. Zhu, Q. Shao, Y. Pi, J. Guo, B. Huang, Y. Qian, X. Huang, *Small*, 13 (2017) 1701295.

13. M. Zhu, B. Huang, Q. Shao, Y. C. Pi, Y. Qian, X. Huang, *ChemCatChem*, 10 (2018) 3214.
14. G.Y. Ren, Q.S. Chen, J.G. Zheng, B. Huang, Y. Qian, *J. Electroanal. Chem.*, 829 (2018) 177.
15. M. Kaempgen, C.K. Chan, J. Ma, Y. Cui, G. Gruner, *Nano Lett*., 9 (2009) 1872.
16. T. Zhu, J. Ding, Q. Shao, Y. Qian, X. Huang, *ChemCatChem*, 11 (2019) 689.
17. G.Y. Ren, Y.N. Li, Q.S. Chen, Y. Qian, J.G. Zheng, Y.A. Zhu, C. Teng, *ACS Sustainable Chem. Eng.*, 6 (2018) 16032.
18. Y. Qian, F. Ye, J. Xu, *Int. J. Electrochem. Sci.*, 7 (2012) 10063.
19. H. Deng, M. Zhu, T. Jin, C. Cheng, J. Zheng, Y. Qian, *Int. J. Electrochem. Sci.*, 15 (2020) 16.
20. X. Qiu, L.M. Lu, J. Leng, Y.F. Yu, W.M. Wang, M. Jiang, L. Bai, *Food Chemistry*, 190 (2016) 889.
21. S.L. Candelariaa, Y.Y. Shao, W. Zhou, X.L. Li, J. Xiao, J.G. Zhang, Y. Wang, J. Liu, J.H. Li, G. Z. Cao, Nano Energy 1 (2012) 195.
22. B. Bayatsarmadi, Y. Zheng, A. Vasileff, S. Z. Qiao, *Small*, 13 (2017) 1700191.
23. C. Yang, I. Sun, C. Hsieh, T. Wu, C. Su, Y. Li, J. Chang, *J. Mater. Chem. A*, 4 (2016) 4015.
24. Y. Qian, C. Huang, R. Chen, S. Dai, C. Wang, *Int. J. Electrochem. Sci.*, 11 (2016) 7453.
25. P. Suktha, N. Phattharasupakun, P. Dittanet, M. Sawangphruk, *RSC Adv.*, 7 (2017) 9958.
26. L. Bao, T. Li, S. Chen, C. Peng, L. Li, Q. Xu, Y. H. Chen, W. J. Xu, *Small*, 13 (2017) 1602077.
27. W. Wang, Q. Hao, W. Lei, X. Xia, X. Wang, *RSC Adv.*, 2 (2012) 10268.
28. L.M. Dai, Y.H. Xue, L.T. Qu, H.J. Choi, J.B. Baek, *Chem. Rev.*, 115 (2015) 4823.
29. X. Yan, Y. Yu, S.K. Ryu, J.L. Lan, X.L. Jia, X.P. Yang, *Electrochimica Acta*, 136 (2014) 466.
30. W. Zhou, J. Wang, F. Zhang, S. Liu, J. Wang, D. Yin, L. Wang, *Chem. Commun.*, 51(2015) 3660.
31. Z. Hou, Y. Jin, X. Xi, T. Huang, D. Wu, P. Xu, R. Liu, *J. Colloid Interface Sci.*, 488(2017) 317.
32. W. Wang, Q. Hao, W. Lei, X. Xia, X. Wang, *RSC Adv.*, 2(2012) 10268.
33. Z. Zhang, L. Wang, J. Xiao, F. Xiao, S. Wang, *ACS Appl. Mater. & Interfaces*, 3 (2015) 17963.
34. Y. Zheng, Y. Jiao, J. Chen, J. Liu, J. Liang, A. Du, W. Zhang, Z. Zhu, M. Jaroniec, G. Lu, S. Qiao, *J. Am. Chem. Soc.*, 133 (2011) 20116.
35. L. Sun, C. Tian, Y. Fu, J. Yin, L. Wang, H. Fu, *Chem. Eur. J.*, 20 (2014) 564.
36. Y. Lin, J. Duh, M. Huang, *J. Phys. Chem. C.*, 114 (2010) 13136.
37. T. Jin, C. Liu, M. Zhou, S. Chai, F. Chen, Q. Fu, *Composites Part A*, 68(2015) 193.
38. T. Jin, J. Chen, C. Wang, Y. Qian, L. Lu, *J. Mater. Sci.*, 55(2020) 12103.
39. J. Xu, J. Huang, M. Zhu, C. Cheng, T. Jin, B. Huang, *Int. J. Electrochem. Sci.*, 15 (2020) 765.
40. S. Ren, Y. Yang, M. Xu, H. Cai, C. Hao, X. Wang, *Colloids Surf. A*, 444(2014) 26.
41. A. A. Yadav, *J. Mater. Sci.*, 27(2016) 1866.
42. V. Vinoth, J. J. Wu, A. M. Asiri, T. Lana-Villarreal, P. Bonete, S. Anandan, *Ultrason. Sonochem.*, 29(2016) 205.
43. T. Fan, C. Huang, R. Chen, J. Xu, C. Wang, Y. Qian, *Int. J. Electrochem. Sci.*, 12(2017) 7659.
44. W. Wang, W. Lei, T. Yao, X. Xia, W. Huang, Q. Hao, X. Wang, *Electrochim. Acta*, 108(2013) 118.
45. C.-H. Xu, J.-Z. Chen, *Ceram. Int.*, 42(2016) 14287.
46. L. Li, P. Gao, S. Gai, F. He, Y. Chen, M. Zhang, P. Yang, *Electrochim. Acta*, 190(2016) 566.